

High throughput thermal conductivity of high temperature solid phases: The case of oxide and fluoride perovskites

Ambroise van Roekeghem,¹ Jesús Carrete,¹ Corey Oses,² Stefano Curtarolo,^{2,3} and Natalio Mingo¹

¹*CEA, LITEN, 17 Rue des Martyrs, 38054 Grenoble, France**

²*Center for Materials Genomics, Duke University, Durham, NC 27708, USA*

³*Materials Science, Electrical Engineering, Physics and Chemistry, Duke University, Durham, NC 27708, USA*

(Dated: June 13, 2016)

Using finite-temperature phonon calculations and machine-learning methods, we calculate the mechanical stability of about 400 semiconducting oxides and fluorides with cubic perovskite structures at 0 K, 300 K and 1000 K. We find 92 mechanically stable compounds at high temperatures – including 36 not mentioned in the literature so far – for which we calculate the thermal conductivity. We demonstrate that the thermal conductivity is generally smaller in fluorides than in oxides, largely due to a lower ionic charge, and describe simple structural descriptors that are correlated with its magnitude. Furthermore, we show that the thermal conductivities of most cubic perovskites decrease more slowly than the usual T^{-1} behavior. Within this set, we also screen for materials exhibiting negative thermal expansion. Finally, we describe a strategy to accelerate the discovery of mechanically stable compounds at high temperatures.

I. INTRODUCTION

High throughput ab-initio screening of materials is a new and rapidly growing discipline [1]. Amongst the basic properties of materials, thermal conductivity is a particularly relevant one. Thermal management is a crucial factor to a vast range of technologies, including power electronics, CMOS interconnects, thermoelectric energy conversion, phase change memories, turbine thermal coatings and many other [2]. Thus, rapid determination of thermal conductivity for large pools of compounds is a desirable goal in itself, which may enable the identification of suitable compounds for targeted applications. A few recent works have investigated thermal conductivity in a high throughput fashion [3, 4]. A drawback of these studies is that they were restricted to use the zero kelvin phonon dispersions. This is often fine when the room temperature phase is mechanically stable at 0 K. It however poses a problem for materials whose room or high temperature phase is not the 0 K structure: when dealing with structures exhibiting displacive distortions, including temperature effects in the phonon spectrum is a crucial necessity.

Such a phenomenon often happens for perovskites. Indeed, the perovskite structure can exhibit several distortions from the ideal cubic lattice, which is often responsible for rich phase diagrams. When the structure is not stable at low temperatures, a simple computation of the phonon spectrum using forces obtained from density functional theory and the finite displacement method yields imaginary eigenvalues. This prevents us from assessing the mechanical stability of those compounds at high temperatures or calculating their thermal conductivity. Moreover, taking into account finite-temperature effects in phonon calculations is currently a very demanding task, especially for a high-throughput investigation.

In this study, we are interested in the *high-temperature*

properties of perovskites, notably for thermoelectric applications. For this reason, we focus on perovskites with the highest symmetry cubic structure, which are most likely to exist at high temperatures [5–9]. We include the effects of anharmonicity in our ab-initio calculations of mechanical and thermal properties.

II. FINITE-TEMPERATURE CALCULATIONS OF MECHANICAL STABILITY AND THERMAL PROPERTIES

Recently, several methods have been developed to deal with anharmonic effects at finite temperatures in solids [10–15]. In this study, we use the method presented in Ref. [15] to compute the temperature-dependent interatomic force constants, which uses a regression analysis of forces from density functional theory coupled with a harmonic model of the quantum canonical ensemble. This is done in an iterative way to achieve self-consistency of the phonon spectrum. The workflow is summarized in Fig. 1. In the following (in particular Section III), it will be referred as “SCFCS” – standing for self-consistent force constants. As a trade-off between accuracy and throughput, we choose a 3x3x3 supercell and a cutoff of 5 Å for the third order force constants. Special attention is paid to the computation of the thermal displacement matrix [15], due to the imaginary frequencies that can appear during the convergence process, as well as the size of the supercell that normally prevents us from sampling the usual soft modes at the corners of the Brillouin zone (see Supplementary Material). This allows us to assess the stability at 1000 K of the 391 hypothetical compounds mentioned in Section I. Among this set, we identify 92 mechanically stable compounds, for which we also check the stability at 300 K. The phonon spectra of the stable compounds are provided in the Supplementary Material.

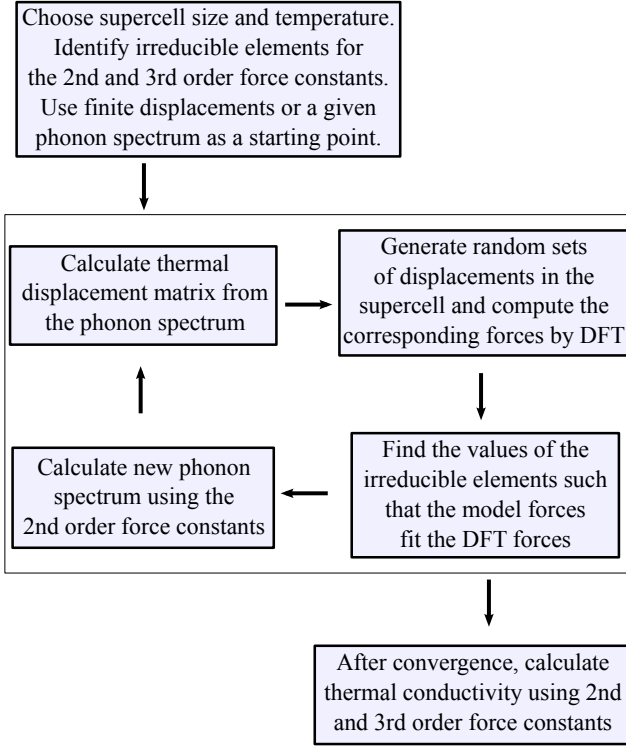


Figure 1. Workflow of the method used to calculate the phonon spectrum and thermal conductivity including finite-temperature anharmonic effects.

Furthermore, we compute the thermal conductivity using the finite temperature force constants and the full solution of the Boltzmann transport equation as implemented in the ShengBTE code [16].

We list the stable compounds and their thermal conductivities in Table I. Remarkably, this list contains 37 perovskites that have been reported experimentally in the ideal cubic structure (see References in Table I), which lends support to our screening method. On the other hand, we also find that 11 compounds are reported only in a non-perovskite form. This is not necessarily indicative of mechanical instability, but instead suggests thermodynamical stability may be an issue for these compounds, at least near this temperature and pressure. 36 compounds remain unreported experimentally in the literature to our knowledge. Thus, by screening only for mechanical stability at high-temperatures, we reduce the number of potential new perovskites by a factor of 10. Furthermore, we find that 50 of them are mechanically stable in the cubic form close to room temperature.

Of the full list of perovskites, only a few measurements of thermal conductivity are available in the literature. They are displayed in parentheses in Table I along with their calculated values. Our method tends to slightly underestimate the value of the thermal conductivity, due to the compromises we made to limit the computational cost of the study (see Supplementary Material). This dis-

crepancy could also be partially related to the electronic thermal conductivity, which was not subtracted in the measurements. Still, we expect the order of magnitude of the thermal conductivity and the relative classification of different materials to be consistent. More importantly, this large dataset allows us to analyze the global trends driving thermal conductivity. These trends are discussed in Section IV.

We also investigate the (potentially) negative thermal expansion of these compounds. Indeed, the sign of the coefficient of thermal expansion α_V is the same as the sign of the weighted Grüneisen parameter γ , following $\alpha_V = \frac{\gamma c_V \rho}{K_T}$, where K_T is the isothermal bulk modulus, c_V is the isochoric heat capacity and ρ is the density [80, 81]. The weighted Grüneisen parameter is obtained by summing the contributions of the mode-dependent Grüneisen parameters: $\gamma = \sum \gamma_i c_{Vi} / \sum c_{Vi}$. Finally the mode-dependent parameters are related to the volume variation of the mode frequency ω_i via $\gamma_i = -(V/\omega_i)(\partial\omega_i/\partial V)$. In our case, we calculate those parameters directly using the second and third order force constants at a given temperature [12, 82, 83]:

$$\gamma_m = -\frac{1}{6\omega_m^2} \sum_{ijk\alpha\beta\gamma} \frac{\epsilon_{mia}^* \epsilon_{mj\beta}}{\sqrt{M_i M_j}} r_k^\gamma \Psi_{ijk}^{\alpha\beta\gamma} e^{i\mathbf{q}\cdot\mathbf{r}_j} \quad (1)$$

This approach has been very successful in predicting the thermal expansion behavior in the empty perovskite ScF_3 [15], which switches from negative to positive around 1100 K [84]. In our list of filled perovskites, we have found only two candidates with negative thermal expansion around room temperature: TlOsF_3 and BeYF_3 , and none at 1000 K. This shows that filling the perovskite structure is probably detrimental to the negative thermal expansion.

We also examine the evolution of the thermal conductivity as a function of temperature, for the compounds that are mechanically stable at 300 K and 1000 K. There is substantial evidence that the thermal conductivity in cubic perovskites generally decreases more slowly than the model $\kappa \propto T^{-1}$ behavior [85, 86] at high temperatures, in contrast to the thermal conductivity of *e.g.* Si or Ge that decreases faster than $\kappa \propto T^{-1}$ [87]. This happens for instance in SrTiO_3 [47, 48], KZnF_3 [21, 76], KMgF_3 [21], KFeF_3 [59], RbCaF_3 [21], BaHfO_3 [31], BaSnO_3 [88] and BaZrO_3 [53]. We also predicted an anomalous behavior in ScF_3 using ab-initio calculations, tracing its origin to the important anharmonicity of the soft modes [15]. Fig. 2 displays several experimentally measured thermal conductivities from the literature on a logarithmic scale, along with the results of our high-throughput calculations. As discussed above, the absolute values of the calculated thermal conductivities are generally underestimated, but their relative magnitude and the overall temperature dependence are generally consistent. Although the behavior of the thermal conductivity $\kappa(T)$ is in general more complex than a simple power-law behavior, we

	κ_{1000}	κ_{300}	Refs.		κ_{1000}	κ_{300}	Refs.		κ_{1000}	κ_{300}	Refs.
CaSiO ₃	4.89		[17]	CdYF ₃	1.29	3.51		TiO ₂ F ₃	0.62	0.95	
RbTaO ₃	3.61		[18]	RbCaF ₃	1.15	2.46 (3.2)	[19–21]	InZnF ₃	0.61	1.86	
NaTaO ₃	3.45		[22]	HgInF ₃	1.15	3.85		CsCdF ₃	0.59	1.73	[23]
CuCF ₃	3.32	8.79	[24]	AlFeF ₃	1.14			AlMgF ₃	0.56		
SrSiO ₃	3.23	10.10	[25]	PbHfO ₃	1.12		[26]	AuZnF ₃	0.53		
NaNbO ₃	3.05	(1.5)	[27–29]	AgMgF ₃	1.11		[30]	InOsF ₃	0.52		
BaHfO ₃	3.04 (4.5)	8.26 (10.4)	[31]	ZnScF ₃	1.10	3.66		RbSrF ₃	0.51		[32]
KNbO ₃	2.94	(10)	[27, 29]	RbFeF ₃	1.09	4.62	[33]	CsSrF ₃	0.50	1.13	[32]
TiTaO ₃	2.86		[34]	TlMgF ₃	1.06	3.42	[35]	BeYF ₃	0.48	2.34	
AgTaO ₃	2.77		[36, 37]	KCaF ₃	1.06		[38]	BeScF ₃	0.48	1.59	
KMgF ₃	2.74	8.25 (10)	[21, 39]	HgScF ₃	1.01	5.42		TlCdF ₃	0.44		[23]
GaTaO ₃	2.63		[40–42]	CsCaF ₃	0.98	3.03	[43]	RbHgF ₃	0.43		[44]
BaTiO ₃	2.51	4.99 (4–5)	[29, 45]	AuMgF ₃	0.96		^a	PdYF ₃	0.43	0.99	
PbTiO ₃	2.42	(5)	[29]	InMgF ₃	0.96	3.53		AlZnF ₃	0.39		
SrTiO ₃	2.36 (4)	6.44 (10.5)	[47–49]	RbZnF ₃	0.91	2.64	[50]	KHgF ₃	0.37		[44]
SrHfO ₃	2.20 (2.7)	(5.2)	[49, 51]	ZnInF ₃	0.88	1.89		RbSnF ₃	0.37	0.82	[52]
BaZrO ₃	2.13 (2.9)	5.61 (5.2)	[53]	BaSiO ₃	0.87		[54]	ZnBiF ₃	0.37	1.29	
XeScF ₃	1.87	4.40		TlCaF ₃	0.86			CsHgF ₃	0.37	1.00	[44]
HgYF ₃	1.84	5.37		CdScF ₃	0.85	2.37		KSrF ₃	0.35		[52]
AgNbO ₃	1.79		[55, 56]	XeBiF ₃	0.82	2.13		CdBiF ₃	0.33	0.98	
TiNbO ₃	1.75		[34]	AgZnF ₃	0.80		[30]	RbPbF ₃	0.32		[57]
KFeF ₃	1.72	6.37 (3.0)	[58, 59]	PdScF ₃	0.79	1.63		BeAlF ₃	0.30	1.70	
SnSiO ₃	1.66	4.22	[60, 61]	KCdF ₃	0.75		[62, 63]	KPbF ₃	0.30		[64]
PbSiO ₃	1.66	3.69	[65, 66]	BaLiF ₃	0.73	2.21	^b [67, 68]	CsBaF ₃	0.29		
AuNbO ₃	1.56		[69]	HgBiF ₃	0.72	2.37		InCdF ₃	0.29		
CaSeO ₃	1.42		[70]	ZnAlF ₃	0.72	1.92		BaCuF ₃	0.28		
NaBeF ₃	1.40	2.53	[71, 72]	GaZnF ₃	0.69			TlSnF ₃	0.27	0.63	[73]
RbMgF ₃	1.37	4.54	[74]	RbCdF ₃	0.68	1.46	[23]	TlHgF ₃	0.26		[75]
GaMgF ₃	1.34	2.11		GaRuF ₃	0.67			CdSbF ₃	0.26		
KZnF ₃	1.33	4.15 (5.5)	[21, 76]	CsZnF ₃	0.67	1.12	[77]	TlPbF ₃	0.22		[78]
ZnYF ₃	1.32	3.72		TlZnF ₃	0.64	1.96	[79]				

^a AuMgF₃ was mentioned theoretically in Ref. [46].

^b The thermal diffusivity of BaLiF₃ was measured at 300 K in Ref. [67] as $\alpha=0.037\text{ cm}^2\text{s}^{-1}$.

Table I. List of cubic perovskites found to be mechanically stable at 1000 K and their corresponding computed lattice thermal conductivity (in W/m/K). We also report the computed lattice thermal conductivity at 300 K (in W/m/K) when we obtain stability at that temperature. We highlight in blue the compounds that are experimentally reported in the ideal cubic perovskite structure, and in red those that are reported only in non-perovskite structures (references provided in the table). When no reference is provided, no mention of the compound in this stoichiometry has been found in the experimental literature. Experimental measurements of the thermal conductivity are reported in parentheses, and in italics when the structure is not cubic.

model the deviation to the $\kappa \propto T^{-1}$ law by using a parameter α that describes approximately the temperature-dependence of κ between 300 K and 1000 K as $\kappa \propto T^{-\alpha}$. For instance, in Fig. 2, KMgF₃ appears to have the fastest decreasing thermal conductivity with $\alpha = 0.9$ both from experiment and calculations, while SrTiO₃ is closer to $\alpha = 0.6$. At present, there are too few experimental measurements of the thermal conductivities in cubic perovskites to state that the $\kappa \propto T^{-\alpha}$ behavior with $\alpha < 1$ is the general rule in this family. However, the large number of theoretical predictions provides a way to assess this trend. Of the 50 compounds that we found to be mechanically stable at room temperature, we find a mean $\alpha \simeq 0.85$, suggesting that this behavior is likely general and correlated to structural characteristics of the perovskites.

III. ACCELERATING THE DISCOVERY OF STABLE COMPOUNDS AT HIGH TEMPERATURE

Through brute-force calculations of the initial list of 391 compounds, we extracted 92 that are mechanically stable at 1000 K. However, this type of calculation is computationally expensive. Thus, it is desirable for future high-throughput searches of other material classes to define a strategy for exploring specific parts of the full combinatorial space. In this section, we propose and test such a strategy based on an iterative machine-learning scheme using principal component analysis and regression.

We begin by calculating the second order force constants Φ_{0K} of all compounds using the finite displacement method, which is more than an order of magnitude

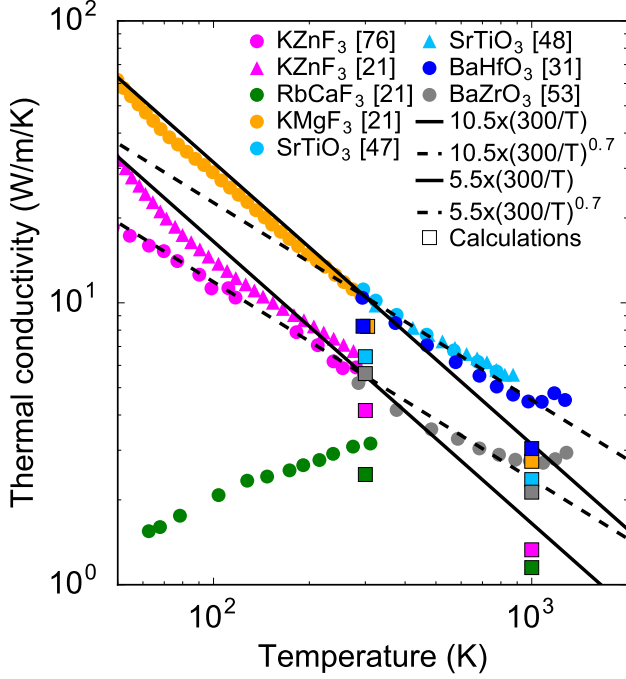


Figure 2. A comparison between total thermal conductivities from Refs. [21, 31, 47, 48, 53, 76], high-throughput calculations of the lattice thermal conductivity at 300 K and 1000 K, and model behaviors in $\kappa \propto T^{-1}$ and $\kappa \propto T^{-0.7}$.

faster than finite-temperature calculations. This gives us a list of 29 perovskites that are mechanically stable in the cubic phase at 0 K. Since this is the highest symmetry phase, they are likely also mechanically stable at high-temperatures [89]. We calculate their self-consistent finite-temperature force constants $\Phi_{1000\text{ K}}^{SCFCS}$ as described in Section II. This initial set allows us to perform principal component analysis of the 0 K force constants so that we obtain a transformation that retains the 10 most important components. In a second step, we use regression analysis to find a relation between the principal components at 0 K and at 1000 K. This finally gives us a model that extracts the principal components of the force constants at 0 K, interpolate their values at 1000 K, and reconstruct the full force constants matrix at 1000 K $\Phi_{1000\text{ K}}^{model}$. We say that this model has been “trained” on the particular set of compounds described above. Applying it to the previously calculated $\Phi_{0\text{ K}}$ for all compounds, we can efficiently span the full combinatorial space to search for new perovskites with a phonon spectrum that is unstable at 0 K but stable at 1000 K. For materials determined mechanically stable with $\Phi_{1000\text{ K}}^{model}$, we calculate $\Phi_{1000\text{ K}}^{SCFCS}$. If the mechanical stability is confirmed, we add the new compound to the initial set and subsequently train the model again with the enlarged set. When no new compounds with confirmed mechanical stability at high temperatures are found, we stop the search. This process is summarized in Figure 3. Following this strat-

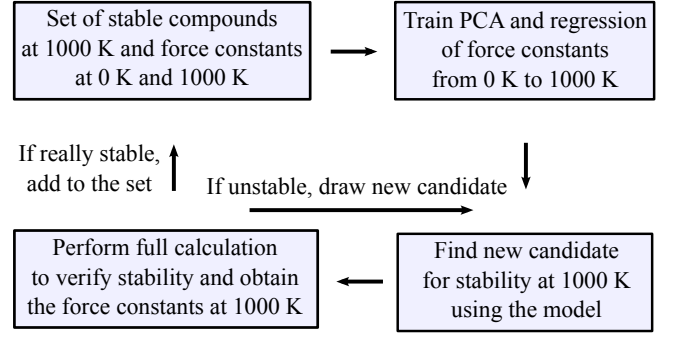


Figure 3. Depiction of strategy for exploring the relevant combinatorial space of compounds that are mechanically stable at high temperature.

egy, we find 79 perovskites that are stable according to the model, 68 of which are confirmed to be stable by the full calculation. This means that we have reduced the total number of finite-temperature calculations by a factor of 5, and that we have retrieved mechanically stable compounds with a precision of 86% and a recall of 74% [90]. It allows us to obtain approximate phonon spectra for unstable compounds, which is not possible with our finite-temperature calculations scheme (see Supplementary Material). It also allows us to find compounds that had not been identified as mechanically stable by the first exhaustive search due to failures in the workflow. Considering the generality of the approach, we expect this method to be applicable to other families of compounds as well. Most importantly, it reduces the computational requirements, particularly if the total combinatorial space is much larger than the space of interest.

IV. SIMPLE DESCRIPTORS OF THE THERMAL CONDUCTIVITY

We now focus on the analysis of the thermal conductivity data provided in Table I. We note that this set contains about two times more fluorides than oxides. This was already the case after the first screening in which we kept only the semiconductors, and it can be explained by the strong electronegativity of fluorine, which generally forms ionic solids with the alkali and alkaline earth metals easily, as well as with elements from groups 12, 13 and 14. This is shown on Fig. 4, in which we display histograms of the columns of elements at sites *A* and *B* of the perovskite in our initial list of paramagnetic semiconductors and after screening for mechanical stability.

We can also see that the oxides tend to display a higher thermal conductivity than the fluorides, as shown on the density plot of Fig. 5. This is once again due to the charge of the fluorine ion, which is half that of the oxygen ion. In a model of a purely ionic solid, this would cause the interatomic forces created by electrostatic interactions to be

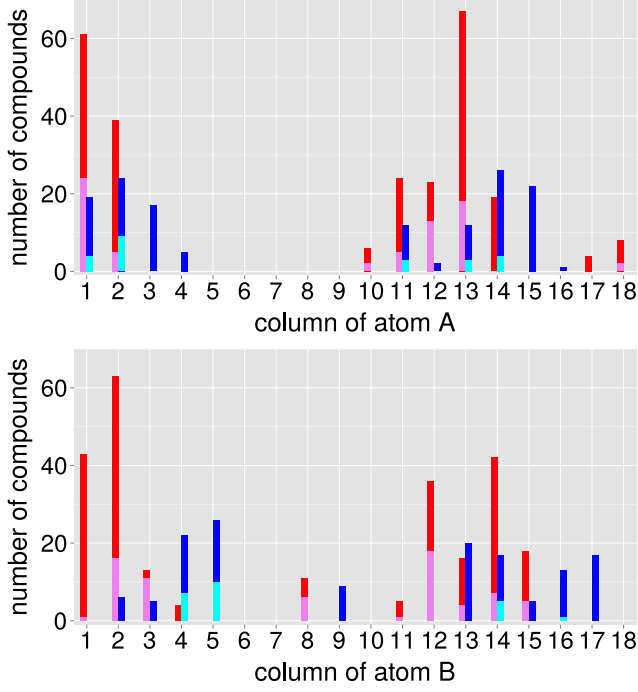


Figure 4. Column number of the element at site A (top) and B (bottom) of the perovskite ABX_3 in the initial list of fluorides (red) and oxides (blue) paramagnetic semiconductors and after screening for mechanical stability (violet and cyan, respectively).

divided by two in fluorides as compared to oxides. This is roughly what we observe in our calculations of the second order force constants. It translates into smaller phonon frequencies and mean group velocities in fluorides as compared to oxides. Fluorides also have smaller heat capacities, due to their larger lattice parameters (see Supplementary material). Those two factors mainly drive the important discrepancy of the thermal conductivity between fluorides and oxides. Following the same reasoning, it means that halide perovskites in general should have a very low thermal conductivity.

Finally, we analyze the correlations between the thermal conductivity and different simple structural descriptors. Fig. 6 displays the correlograms for fluorides and oxides between the following variables: the thermal conductivity κ , the thermal conductivity in the small grain limit κ_{sg} [3, 91], the mean phonon group velocity v_g , the heat capacity c_V , the root mean square Grüneisen parameter γ_{rms} [92, 93], the masses of atoms at sites A and B of the perovskite ABX_3 , their electronegativity, their Petti-for number [94], their ionic radius, the lattice parameter of the compound and its electronic gap. Remarkably, sites A and B play very different roles in fluorides and oxides. In particular, the thermal conductivity of fluorides is mostly influenced by substitutions of the atom inside the fluorine octahedron (site B), while the interstitial atom at site A has a negligible impact. The opposite

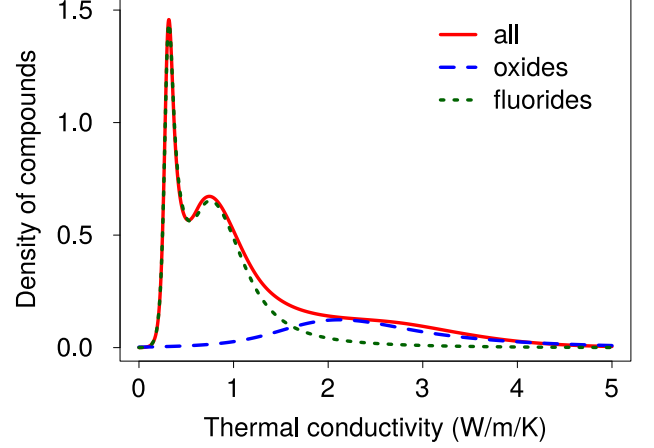


Figure 5. Distribution of compounds as a function of the lattice thermal conductivity at 1000 K. The red curve corresponds to the distribution for all mechanically stable compounds. The blue curve corresponds to the distribution for fluorides only. The green curve corresponds to the distribution for oxides only.

is true for the oxides. This means that when searching for new compounds with a low lattice thermal conductivity, substitutions at the A site of fluorides can be performed to optimize cost or other considerations without impacting thermal transport. It is also interesting to note that the gap is largely correlated with the electronegativity of atom B , suggesting the first electronic excitations likely involve electron transfer from the anion to the B atom.

Common to both fluorides and oxides, the lattice parameter is mostly correlated with the ionic radius of atom B rather than atom A . Interestingly, the lattice parameter is larger for fluorides, although the ionic radius of fluorine is smaller than for oxygen. This is presumably due to partially covalent bonding in oxides (see e.g. Ref. 95). In contrast, fluorides are more ionic: the mean degree of ionicity of the X - B bond calculated from Pauling's electronegativities [96] e_X and e_B as $I_{XB} = 100 (1 - e^{(e_X - e_B)/4})$ yields a value of 56% for oxides versus 74% for fluorides. Ionicity is also reflected by the band structure, as can be seen from the weak dispersion and hybridization of the F-2p bands [97]. This may explain why the role of atoms at site A and B is so different between the two types of perovskites. We think that the more ionic character combined to the small nominal charge in fluorides makes the octahedron cage enclosing the atom B less rigid, such that the influence of the atom B on the thermal conductivity becomes more significant.

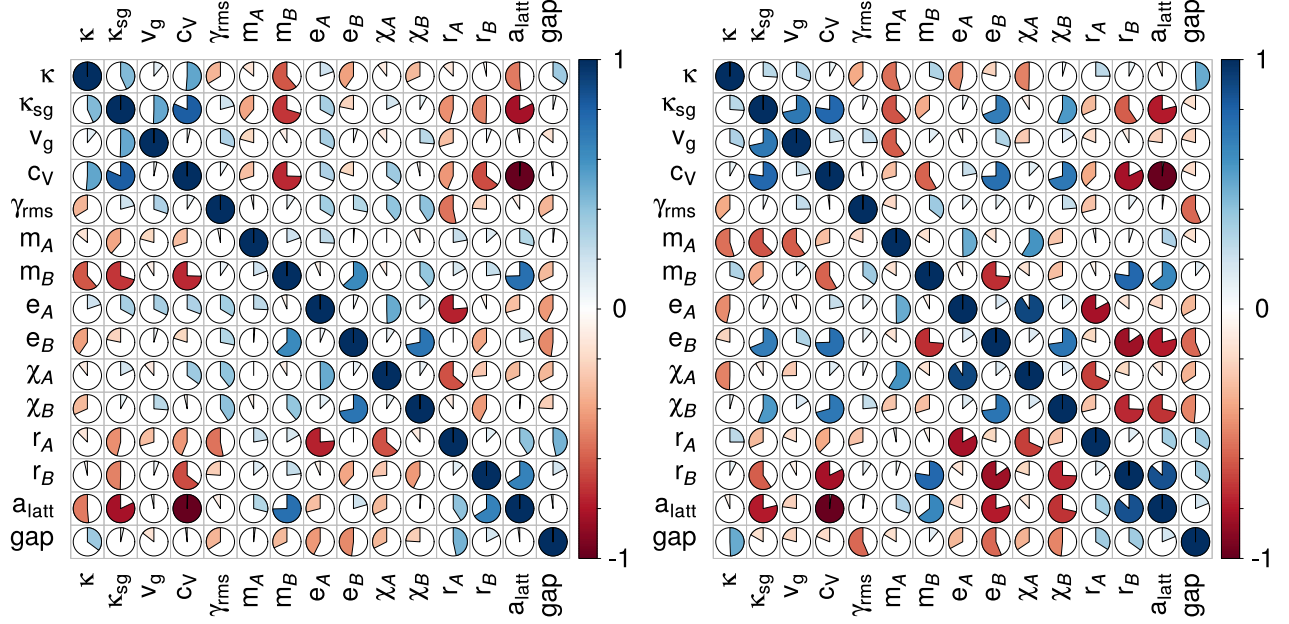


Figure 6. Correlograms between the thermal conductivity κ , the thermal conductivity in the small grain limit κ_{sg} , the mean phonon group velocity v_g , the heat capacity c_v , the root mean square Grüneisen parameter γ_{rms} , the masses m_A and m_B of atoms at sites A and B of the perovskite ABX_3 , their electronegativity e_A , e_B , their Pettifor scale χ_A , χ_B , their ionic radius r_A , r_B , the lattice parameter of the compound a_{latt} and its electronic gap, for mechanically stable fluorides (left) and oxides (right) at 1000 K.

V. CONCLUSION

Employing finite-temperature *ab-initio* calculations of force constants in combination with machine learning techniques, we have assessed the mechanical stability and thermal conductivity of hundreds of oxides and fluorides with cubic perovskite structures at high temperatures. We have shown that the thermal conductivities of fluorides are generally much smaller than those of oxides, and we found new potentially stable perovskite compounds. We have also shown that the thermal conductivity of cubic perovskites generally decreases more slowly than the inverse of temperature. Finally, we provide simple ways of tuning the thermal properties of oxides and fluorides by contrasting the effects of substitutions at the A and B sites. We hope that this work will trigger further interest in halide perovskites for applications that require a low thermal conductivity.

This work is partially supported by the French “Carnot” project SIEVE. C. Oses acknowledges support from the National Science Foundation Graduate Research Fellowship under Grant No. DGF1106401. We also acknowledge the CRAY corporation for computational support.

* ambroise.van-roekeghem@polytechnique.edu

- [1] S. Curtarolo, G. L. Hart, M. B. Nardelli, N. Mingo, S. Sanvito, and O. Levy, “The high-throughput highway to computational materials design,” *Nat. Mater.* **12**, 191–201 (2013).
- [2] D. G. Cahill, P. V. Braun, G. Chen, D. R. Clarke, S. Fan, K. E. Goodson, P. Keblinski, W. P. King, G. D. Mahan, A. Majumdar, H. J. Maris, S. R. Phillpot, E. Pop, and L. Shi, “Nanoscale thermal transport. II. 2003–2012,” *Appl. Phys. Rev.* **1**, 011305 (2014).
- [3] J. Carrete, W. Li, N. Mingo, S. Wang, and S. Curtarolo, “Finding Unprecedentedly Low-Thermal-Conductivity Half-Heusler Semiconductors via High-Throughput Materials Modeling,” *Phys. Rev. X* **4**, 011019 (2014).
- [4] A. Seko, A. Togo, H. Hayashi, K. Tsuda, L. Chaput, and I. Tanaka, “Prediction of Low-Thermal-Conductivity Compounds with First-Principles Anharmonic Lattice-Dynamics Calculations and Bayesian Optimization,” *Phys. Rev. Lett.* **115**, 205901 (2015).
- [5] L. D. Landau and E. M. Lifshitz, *Course of theoretical physics*, Vol. 5 (Pergamon Press, 1969).
- [6] C. J. Howard and H. T. Stokes, “Structures and phase transitions in perovskites – a group-theoretical approach,” *Acta Cryst. A* **61**, 93–111 (2005).
- [7] H. Thomas and K. A. Müller, “Structural Phase Transitions in Perovskite-Type Crystals,” *Phys. Rev. Lett.* **21**, 1256–1259 (1968).

- [8] W. Cochran and A. Zia, “Structure and dynamics of perovskite-type crystals,” *Phys. Status Solidi B* **25**, 273–283 (1968).
- [9] R. J. Angel, J. Zhao, and N. L. Ross, “General Rules for Predicting Phase Transitions in Perovskites due to Octahedral Tilting,” *Phys. Rev. Lett.* **95**, 025503 (2005).
- [10] P. Souvatzis, O. Eriksson, M. I. Katsnelson, and S. P. Rudin, “Entropy Driven Stabilization of Energetically Unstable Crystal Structures Explained from First Principles Theory,” *Phys. Rev. Lett.* **100**, 095901 (2008).
- [11] O. Hellman, I. A. Abrikosov, and S. I. Simak, “Lattice dynamics of anharmonic solids from first principles,” *Phys. Rev. B* **84**, 180301 (2011).
- [12] O. Hellman and I. A. Abrikosov, “Temperature-dependent effective third-order interatomic force constants from first principles,” *Phys. Rev. B* **88**, 144301 (2013).
- [13] I. Errea, M. Calandra, and F. Mauri, “First-Principles Theory of Anharmonicity and the Inverse Isotope Effect in Superconducting Palladium-Hydride Compounds,” *Phys. Rev. Lett.* **111**, 177002 (2013).
- [14] T. Tadano and S. Tsuneyuki, “Self-consistent phonon calculations of lattice dynamical properties in cubic SrTiO_3 with first-principles anharmonic force constants,” *Phys. Rev. B* **92**, 054301 (2015).
- [15] A. van Roekeghem, J. Carrete, and N. Mingo, “Anomalous thermal conductivity and suppression of negative thermal expansion in ScF_3 ,” [arXiv:1601.00561](https://arxiv.org/abs/1601.00561) (2016).
- [16] W. Li, J. Carrete, N. A. Katcho, and N. Mingo, “ShengBTE: a solver of the Boltzmann transport equation for phonons,” *Comp. Phys. Commun.* **185**, 1747–1758 (2014).
- [17] T. Komabayashi, K. Hirose, N. Sata, Y. Ohishi, and L. S. Dubrovinsky, “Phase transition in CaSiO_3 perovskite,” *Earth Planet. Sci. Lett.* **260**, 564 – 569 (2007).
- [18] A. I. Lebedev, “Ferroelectric properties of RbNbO_3 and RbTaO_3 ,” *Phys. Solid State* **57**, 331–336 (2015).
- [19] W. L. W. Ludekens and A. J. E. Welch, “Reactions between metal oxides and fluorides: some new double-fluoride structures of type ABF_3 ,” *Acta Cryst.* **5**, 841 (1952).
- [20] C. Ridou, M. Rousseau, J. Y. Gesland, J. Nouet, and A. Zarembowitch, “The 193 K phase transition in RbCaF_3 ,” *Ferroelectrics* **12**, 199–200 (1976).
- [21] J. Martin, “Thermal Conductivity of RbCaF_3 ,” in *Phonon Scattering in Solids*, edited by L. Challis, V. Rampton, and A. Wyatt (Springer US, 1976) pp. 258–260.
- [22] B. J. Kennedy, A. K. Prodjosantoso, and C. J. Howard, “Powder neutron diffraction study of the high temperature phase transitions in NaTaO_3 ,” *J. Phys.: Condens. Matter* **11**, 6319 (1999).
- [23] M. Rousseau, J. Y. Gesland, J. Julliard, J. Nouet, J. Zarembowitch, and A. Zarembowitch, “Crystallographic, elastic, and Raman scattering investigations of structural phase transitions in RbCdF_3 and TlCdF_3 ,” *Phys. Rev. B* **12**, 1579–1590 (1975).
- [24] A. Zanardi, M. A. Novikov, E. Martin, J. Benet-Buchholz, and V. V. Grushin, “Direct Cupration of Fluoroform,” *J. Am. Chem. Soc.* **133**, 20901–20913 (2011).
- [25] W. Xiao, D. Tan, W. Zhou, J. Liu, and J. Xu, “Cubic perovskite polymorph of strontium metasilicate at high pressures,” *Am. Mineral.* **98**, 2096–2104 (2013).
- [26] J. Kwapulinski, M. Pawełczyk, and J. Dec, “On the Pb thermal vibrations in PbHfO_3 crystals,” *J. Phys.: Condens. Matter* **6**, 4655 (1994).
- [27] G. Shirane, R. Newnham, and R. Pepinsky, “Dielectric Properties and Phase Transitions of NaNbO_3 and $(\text{Na},\text{K})\text{NbO}_3$,” *Phys. Rev.* **96**, 581–588 (1954).
- [28] S. K. Mishra, R. Mittal, V. Y. Pomjakushin, and S. L. Chaplot, “Phase stability and structural temperature dependence in sodium niobate: A high-resolution powder neutron diffraction study,” *Phys. Rev. B* **83**, 134105 (2011).
- [29] M. Tachibana, T. Kolodiazny, and E. Takayama-Muromachi, “Thermal conductivity of perovskite ferroelectrics,” *Appl. Phys. Lett.* **93**, 092902 (2008).
- [30] J. Portier, A. Tressaud, and J.-L. Dupin, “Les pérovskites fluorées AgMeF_3 ($\text{Me} = \text{Mg}, \text{Mn}, \text{Co}, \text{Ni}, \text{Cu}, \text{Zn}$),” *Cr. Acad. Sci. C* **270**, 216–218 (1970).
- [31] T. Maekawa, K. Kurosaki, and S. Yamanaka, “Thermal and mechanical properties of perovskite-type barium hafnate,” *J. Alloy. Compd.* **407**, 44 – 48 (2006).
- [32] W. Pies and A. Weiss, “a566, I.1.3 Complex fluorides and fluorine double salts,” in *Key Elements: F, Cl, Br, I* (Springer Science Business Media, 1973) pp. 104–115.
- [33] M. Kestigian, F. D. Leipziger, W. J. Croft, and R. Guidoboni, “Preparation, Single Crystal Growth, and Crystallographic Properties of FeF_2 , RbFeF_3 , and CsFeF_3 ,” *Inorg. Chem.* **5**, 1462–1463 (1966).
- [34] N. Ramadass, T. Palanisamy, J. Gopalakrishnan, G. Aravamudan, and M. Sastri, “Some ABO_3 oxides with defect pyrochlore structure,” *Solid State Commun.* **17**, 545 – 547 (1975).
- [35] M. Arakawa, A. Okamoto, H. Ebisu, and H. Takeuchi, “An electron paramagnetic resonance study of Fe^{3+} centres in Tl_2MgF_4 and Tl_2ZnF_4 crystals,” *J. Phys.: Condens. Matter* **18**.
- [36] A. Kania and A. Ratuszna, “Phase transitions in AgTaO_3 single crystals,” *Phase Transit.* **2**, 7–13 (1981).
- [37] M. Pawełczyk, “Phase transitions in $\text{AgTa}_x\text{Nb}_{1-x}\text{O}_3$ solid solutions,” *Phase Transit.* **8**, 273–292 (1987).
- [38] D. Demetriou, C. Catlow, A. Chadwick, G. McIntyre, and I. Abrahams, “The anion disorder in the perovskite fluoride KCaF_3 ,” *Solid State Ionics* **176**, 1571 – 1575 (2005).
- [39] I. G. Wood, K. S. Knight, G. D. Price, and J. A. Stuart, “Thermal expansion and atomic displacement parameters of cubic KMgF_3 perovskite determined by high-resolution neutron powder diffraction,” *J. Appl. Crystallogr.* **35**, 291–295 (2002).
- [40] J. Xu, *The low temperature synthesis, characterization and properties of ferroelectrics*, Ph.D. thesis, Georgia Institute of Technology (2000).
- [41] R. Armiento, B. Kozinsky, M. Fornari, and G. Ceder, “Screening for high-performance piezoelectrics using high-throughput density functional theory,” *Phys. Rev. B* **84**, 014103 (2011).
- [42] I. E. Castelli, T. Olsen, S. Datta, D. D. Landis, S. Dahl, K. S. Thygesen, and K. W. Jacobsen, “Computational screening of perovskite metal oxides for optimal solar light capture,” *Energy Environ. Sci.* **5**, 5814–5819 (2012).
- [43] M. Rousseau, J. Gesland, B. Hennion, G. Heger, and B. Renker, “Low energy phonon dispersion curves of KZnF_3 and CsCaF_3 ,” *Solid State Commun.* **38**, 45 – 47 (1981).

- [44] R. Hoppe and R. Homann, “Über CsHgF_3 , RbHgF_3 und KHgF_3 ,” *Z. Anorg. Allg. Chem.* **369**, 212–216 (1969).
- [45] B. A. Strukov, S. T. Davitadze, S. N. Kravchun, S. A. Taraskin, M. Goltzman, V. V. Lemanov, and S. G. Shulman, “Specific heat and heat conductivity of BaTiO_3 polycrystalline films in the thickness range 20–1100 nm,” *J. Phys.: Condens. Matter* **15**, 4331 (2003).
- [46] Y. Uetsuji, S. Kumazawa, T. Ohnishi, K. Tsuchiya, and E. Nakamachi, “Structure Evaluation of Bio-Compatible Lead-Free Piezoelectric Materials by Crystal System Distinction and First Principles Calculations,” *T. Jpn. Soc. Mec. Eng.* **A72**, 1472–1478 (2006).
- [47] H. Muta, K. Kurosaki, and S. Yamanaka, “Thermoelectric properties of reduced and La-doped single-crystalline SrTiO_3 ,” *J. Alloy. Compd.* **392**, 306 – 309 (2005).
- [48] S. R. Popuri, A. J. M. Scott, R. A. Downie, M. A. Hall, E. Suard, R. Decourt, M. Pollet, and J.-W. G. Bos, “Glass-like thermal conductivity in SrTiO_3 thermoelectrics induced by A-site vacancies,” *RSC Adv.* **4**, 33720–33723 (2014).
- [49] S. Yamanaka, T. Maekawa, H. Muta, T. Matsuda, S.-i. Kobayashi, and K. Kurosaki, “Thermophysical properties of SrHfO_3 and SrRuO_3 ,” *J. Solid State Chem.* **177**, 3484 – 3489 (2004).
- [50] P. Daniel, J. Toulouse, J. Y. Gesland, and M. Rousseau, “Raman-scattering investigation of the hexagonal perovskite RbZnF_3 ,” *Phys. Rev. B* **52**, 9129–9132 (1995).
- [51] B. J. Kennedy, C. J. Howard, and B. C. Chakoumakos, “High-temperature phase transitions in SrHfO_3 ,” *Phys. Rev. B* **60**, 2972–2975 (1999).
- [52] T. Thao Tran and P. Shiv Halasyamani, “Synthesis and characterization of ASnF_3 ($A=\text{Na}^+$, K^+ , Rb^+ , Cs^+),” *J. Solid State Chem.* **210**, 213 – 218 (2014).
- [53] S. Yamanaka, T. Hamaguchi, T. Oyama, T. Matsuda, S.-i. Kobayashi, and K. Kurosaki, “Heat capacities and thermal conductivities of perovskite type BaZrO_3 and BaCeO_3 ,” *J. Alloy. Compd.* **359**, 1 – 4 (2003).
- [54] H. Yusa, N. Sata, and Y. Ohishi, “Rhombohedral (9R) and hexagonal (6H) perovskites in barium silicates under high pressure,” *Am. Mineral.* **92**, 648–654 (2007).
- [55] M. Łukaszewski, M. Pawełczyk, J. Hańderek, and A. Kania, “On the phase transitions in silver niobate AgNbO_3 ,” *Phase Transit.* **3**, 247–257 (1983).
- [56] P. Sciau, A. Kania, B. Dkhil, E. Suard, and A. Ratuszna, “Structural investigation of AgNbO_3 phases using X-ray and neutron diffraction,” *J. Phys.: Condens. Matter* **16**, 2795 (2004).
- [57] Y. Yamane, K. Yamada, and K. Inoue, “Mechanochemical synthesis and order–disorder phase transition in fluoride ion conductor RbPbF_3 ,” *Solid State Ionics* **179**, 605 – 610 (2008).
- [58] A. Okazaki and Y. Suemune, “The Crystal Structures of KMnF_3 , KFeF_3 , KCoF_3 , KNiF_3 and KCuF_3 above and below their Néel Temperatures,” *J. Phys. Soc. Jpn.* **16**, 671–675 (1961).
- [59] Y. Suemune, “The Anomalous Thermal Conduction in KFeF_3 Single Crystal at Low Temperatures,” *J. Phys. Soc. Jpn.* **19**, 2234–2234 (1964).
- [60] B. L. Clark and D. A. Keszler, “Hydrothermal Dehydration of Precipitates: Convenient Synthesis Method for Solids,” *Inorg. Chem.* **40**, 1724–1725 (2001).
- [61] R. Armiento, B. Kozinsky, G. Hautier, M. Fornari, and G. Ceder, “High-throughput screening of perovskite alloys for piezoelectric performance and thermodynamic stability,” *Phys. Rev. B* **89**, 134103 (2014).
- [62] M. Hidaka, S. Hosogi, M. Ono, and K. Horai, “Structural phase transitions in KCdF_3 ,” *Solid State Commun.* **23**, 503 – 506 (1977).
- [63] M. Hidaka, Z. Zhou, and S. Yamashita, “Structural phase transitions in KCdF_3 and $\text{K}_{0.5}\text{Rb}_{0.5}\text{CdF}_3$,” *Phase Transit.* **20**, 83–94 (1990).
- [64] S. Hull and P. Berastegui, “Superionic phases in the $(\text{PbF}_2)_{1-x}(\text{MF})_x$, $M = \text{K}, \text{Rb}$ and Cs , systems,” *J. Phys.: Condens. Matter* **11**, 5257 (1999).
- [65] A. Mackay, “The unit cell and space-group of alamosite (PbSiO_3),” *Mineral. Mag* **29**, 933–935 (1952).
- [66] W. Xiao, D. Tan, W. Zhou, M. Chen, X. Xiong, M. Song, J. Liu, H.-K. Mao, and J. Xu, “A new cubic perovskite in PbGeO_3 at high pressures,” *Am. Mineral.* **97**, 1193–1198 (2012).
- [67] M. Duarte, M. Vieira, and S. Baldochi, “Thermal diffusivity of BaLiF_3 crystals,” *Mat. Sci. Eng. B* **25**, 133 – 134 (1994).
- [68] M. Mortier, J. Gesland, and M. Rousseau, “Experimental and theoretical study of second-order Raman scattering in BaLiF_3 ,” *Solid State Commun.* **89**, 369 – 371 (1994).
- [69] X.-N. Wu, X.-N. Li, X.-L. Ding, and S.-G. He, “Activation of Multiple C–H Bonds Promoted by Gold in AuNbO_3^+ Clusters,” *Angew. Chem. Int. Ed.* **52**, 2444–2448 (2013).
- [70] M. Wildner and G. Giester, “Crystal structures of SrSeO_3 and CaSeO_3 and their respective relationships with molybdomenite- and monazite-type compounds – an example for stereochemical equivalence of ESeO_3 groups ($E = \text{lone electron pair}$) with tetrahedral TO_4 groups,” *Neues Jb. Miner. Abh.* **184**, 29–37 (2007).
- [71] H. O’Daniel and L. Tscheischwili, “Zur Struktur von NaBeF_3 und $\beta\text{-CaSiO}_3$,” *Neues Jb. Miner. Abh.* **1945–1948**, 56 (1945).
- [72] D. M. Roy, R. Roy, and E. F. Osborn, “Fluoride Model Systems: III, The System NaF–BeF_2 and the Polymorphism of Na_2BeF_4 and BeF_2 ,” *J. Am. Ceram. Soc.* **36**, 185–190 (1953).
- [73] J. Foulon, J. Durand, A. Larbot, L. Cot, and A. Soufiane, “Crystal Structures of MSnF_3 for $M: \text{K}, \text{Rb}, \text{Tl}$; Ionic Mobility,” *Eur. J. Solid State Inorg. Chem.* **30**, 87–99 (1993).
- [74] M. Shafer and T. McGuire, “Preparation and properties of ferrimagnets in the $\text{RbMgF}_3\text{–RbCoF}_3$ system,” *J. Phys. Chem. Solids* **30**, 1989 – 1997 (1969).
- [75] C. Hebecker, “Neue ternäre Fluoride mit einwertigem Thallium und Silber als Kationen,” *Naturwiss.* **60**, 154–154 (1973).
- [76] Y. Suemune and H. Ikawa, “Thermal Conductivity of KMnF_3 , KCoF_3 , KNiF_3 , and KZnF_3 Single Crystals,” *J. Phys. Soc. Jpn.* **19**, 1686–1690 (1964).
- [77] J. Longo and J. Kafalas, “The effect of pressure and B-cation size on the crystal structure of CsBF_3 compounds ($B=\text{Mn}, \text{Fe}, \text{Co}, \text{Ni}, \text{Zn}, \text{Mg}$),” *J. Solid State Chem.* **1**, 103 – 108 (1969).
- [78] I. I. Buchinskaya and P. P. Fedorov, “Lead difluoride and related systems,” *Russ. Chem. Rev.* **73**, 371 (2004).
- [79] D. Babel, “Structure and Bonding,” (Springer Berlin Heidelberg, Berlin, Heidelberg, 1967) Chap. Structural chemistry of octahedral fluorocomplexes of the transition elements, pp. 1–87.

- [80] E. Grüneisen, “*Theorie des festen Zustandes einatomiger Elemente*,” *Ann. Physik* **344**, 257–306 (1912).
- [81] N. Ashcroft and N. Mermin, *Solid State Physics* (Saunders College, Philadelphia, 1976).
- [82] J. Fabian and P. B. Allen, “*Thermal Expansion and Grüneisen Parameters of Amorphous Silicon: A Realistic Model Calculation*,” *Phys. Rev. Lett.* **79**, 1885–1888 (1997).
- [83] D. A. Broido, A. Ward, and N. Mingo, “*Lattice thermal conductivity of silicon from empirical interatomic potentials*,” *Phys. Rev. B* **72**, 014308 (2005).
- [84] B. K. Greve, K. L. Martin, P. L. Lee, P. J. Chupas, K. W. Chapman, and A. P. Wilkinson, “*Pronounced Negative Thermal Expansion from a Simple Structure: Cubic ScF_3* ,” *J. Am. Chem. Soc.* **132**, 15496–15498 (2010).
- [85] R. Peierls, “*Zur kinetischen Theorie der Wärmeleitung in Kristallen*,” *Ann. Phys. (Leipzig)* **3**, 1055–1101 (1929).
- [86] M. C. Roufosse and P. G. Klemens, “*Lattice thermal conductivity of minerals at high temperatures*,” *J. Geophys. Res.* **79**, 703–705 (1974).
- [87] C. J. Glassbrenner and G. A. Slack, “*Thermal Conductivity of Silicon and Germanium from 3° K to the Melting Point*,” *Phys. Rev.* **134**, A1058–A1069 (1964).
- [88] T. Maekawa, K. Kurosaki, and S. Yamanaka, “*Thermal and mechanical properties of polycrystalline BaSnO_3* ,” *J. Alloy. Compd.* **416**, 214 – 217 (2006).
- [89] However, we note that transitions to other structures can take place, in particular with one of hexagonal symmetry, such as in BaTiO_3 [98], RbZnF_3 [50] or RbMgF_3 [74]. This phase transition is of first order, in contrast to displacive transitions that are of second order.
- [90] Precision is defined as the fraction of true positives in all positives reported by the model and recall as the fraction of true positives found using the model with respect to all true positives.
- [91] J. Carrete, N. Mingo, S. Wang, and S. Curtarolo, “*Nanograined Half-Heusler Semiconductors as Advanced Thermoelectrics: An Ab Initio High-Throughput Statistical Study*,” *Adv. Funct. Mater.* **24**, 7427–7432 (2014).
- [92] L. Bjerg, B. B. Iversen, and G. K. H. Madsen, “*Modeling the thermal conductivities of the zinc antimonides ZnSb and Zn_4Sb_3* ,” *Phys. Rev. B* **89**, 024304 (2014).
- [93] G. K. H. Madsen, A. Katre, and C. Bera, “*Calculating the thermal conductivity of the silicon clathrates using the quasi-harmonic approximation*,” *Phys. Status Solidi A* **213**, 802–807 (2016).
- [94] D. Pettifor, “*A chemical scale for crystal-structure maps*,” *Solid State Commun.* **51**, 31 – 34 (1984).
- [95] A. Kozłowski and K. Tkacz-Śmiech, “*From the Molecular Picture to the Band Structure of Cubic and Tetragonal Barium Titanate*,” *Ferroelectrics* **314**, 123–134 (2005).
- [96] L. Pauling, “*The nature of the chemical bond. IV. The energy of single bonds and the relative electronegativity of atoms*,” *J. Am. Chem. Soc.* **54**, 3570–3582 (1932).
- [97] See for instance the band structure of SrTiO_3 [99] compared to the one of KCaF_3 [100]. In those two compounds, the degree of ionicity of the $X\text{-B}$ bond calculated from Pauling’s electronegativity is 59% and 89%, respectively.
- [98] R. M. Glaister and H. F. Kay, “*An Investigation of the Cubic-Hexagonal Transition in Barium Titanate*,” *Proc. Phys. Soc.* **76**, 763 (1960).
- [99] K. van Benthem, C. Elsässer, and R. H. French, “*Bulk electronic structure of SrTiO_3 : Experiment and theory*,” *J. Appl. Phys.* **90**, 6156–6164 (2001).
- [100] B. Ghebouli, M. Fatmi, M. Ghebouli, H. Choutri, L. Louail, T. Chihi, A. Bouhemadou, and S. Bin-Omran, “*Theoretical study of the structural, elastic, electronic and optical properties of XCuF_3 ($X = \text{K}$ and Rb)*,” *Solid State Sci.* **43**, 9 – 14 (2015).